OPTICAL PARAMETERS OF InP-BASED WAVEGUIDES

F. FIEDLER† and A. SCHLACHETZKI†

Institut für Hochfrequenztechnik, Technische Universität Braunschweig, D-3300 Braunschweig, W. Germany

(Received 6 January 1986; in revised form 8 May 1986)

Abstract—The quaternary alloys InGaAsP, matched in their lattice constant to InP, are considered in view of optical-waveguide applications. The parameters, most important in this connexion, are the refractive index n and the optical absorption coefficient α . Both are calculated starting from quantities relevant to the binary constituents of the system InGaAsP. The results are compared with the relatively few experiments reported in the literature. The calculations are applied to film and rectangular waveguides, showing that they are sufficiently low in loss for integrated-optics applications.

Optical communication systems using glass fibers are now well advanced so that they are employed on a large scale[1]. It is almost generally accepted that single-mode fibers will serve as the transmission medium even in the subscriber network, since they offer the greatest potential with respect to bandwidth and upgrade capability[2]. This application then requires the mass production of the electronic and electro-optic circuits to be used within the optical communication systems, because low cost and high reliability are of prime concern. Consequently, integrated optoelectronics and, more generally, integrated optics are of rapidly growing importance, since only these techniques promise to meet the requirements mentioned before. Particularly if coherent transmission will have matured to the point of extended practical use, then integrated optics will become indispensable.

Integrated optical circuits, to be used with wavelength-division multiplexing techniques or coherent transmission, comprise as key components optical waveguides in addition to electronic and optoelectronic devices. Thus it is essential to have a thorough understanding of the optical parameters controlling the waveguide performance. They are basically the refractive index n and the optical absorption coefficient α .

The materials presently at hand for waveguide fabrication are glass or quartz, lithium niobate and tantalate as well as III-V semiconductors such as GaAlAs/GaAs, InGaAsP/InP and possibly InGaAlAs/InP. For the longer wavelength range one might also think of II-VI compounds like HgCdTe. Glass and quartz can only be used for passive components, e.g. waveguides or couplers. Because of the occurrence of the electro-optic effect, modulators and switches can be made from the lithium compounds in

†Present address: Heinrich-Hertz-Institut, Einsteinufer 37, D-1000 Berlin 10, W. Germany.

addition to the passive components. Whereas the III-V semiconductors provide all the functions mentioned so far, they offer a much wider potential in that they are the basis for numerous electronic and optoelectronic devices. The quaternary system In-GaAsP, matched in its composition to the lattice constant of InP, is certainly the most important semiconductor for the present application[3].

After some more general considerations on the choice of semiconductor materials, InGaAsP/InP is discussed in this paper in view of the design of optical waveguides. By comparison with available experimental data we will find out which interpolation scheme is best suited to describe material properties like n within the composition range of InGaAsP relevant to waveguides. We will describe which minimum value of α , the most important limiting factor to waveguide performance, can be expected. Finally, we will compare waveguide structures with each other which can be relatively easily fabricated with known technologies.

1. MATERIAL CONSIDERATIONS

Optoelectronic devices will find large-scale application in optical communication systems utilizing silica fibers with their optimum wavelength range near 1.3 and $1.5 \mu m$. This precludes GaAs-based semiconductors which instead will be used extensively with applications like optical discs in the shorter wavelength regime. Thus InGaAsP remains as the principal candidate for the longer wavelength range. Consequently this material system has been thoroughly investigated[3].

Optical waveguides as indispensable components in integrated optical circuits are characterized by their necessarily large length (typically at least several hundred μ m) so that they consume a considerable portion of the semiconductor area, even if mirrors are to be used to reduce the length of bends[4]. Therefore

material cost has to be taken into consideration when conceiving integrated optical circuits on semiconductor basis. At present GaAs is at least one order of magnitude more expensive than Si, although there are good prospects of a reduction of this factor when GaAs eventually finds truely large-volume applications. The price of InP is presently 3-5 times higher than that of GaAs. It is likely that the difference between InP and GaAs will endure in the future, because the source materials of InP are more expensive and rare and because InP is more difficult to pull as single crystal than GaAs. Consequently, although absolutely necessary, waveguides will be confined to the most essential functions in integrated optical circuits. Along with the waveguides, all electronic and optoelectronic functions can be monolithically integrated on HI-V semiconductors. This is their main advantage as compared to the competing dielectric materials.

Optical waveguides with InGaAsP can be designed by controlling the refractive index n by proper choice of the composition. Experimental data on the variation of n with composition and wavelength are available [5–7]. An alternative is to guide the light by free-carrier-concentration profiles or by mechanical stress [8]. Whereas all these methods are permanent, n can be varied by exploiting the electro-optic effect [9] as demonstrated by experiment [10]. At the expense of large power dissipation n can be influenced by the injection of free carriers. Optical switches were realized by this technique [11].

Optical absorption is usually detrimental to waveguide performance so that a minimum value of the absorption coefficient α is aimed at. In the following we will discuss in detail which causes are of influence on α . However, we will not go into the Franz-Keldysh effect[12], which allows the variable control of α .

2. INTERPOLATION SCHEMES

For the present application the best suited material is the quaternary semiconductor $In_{1-x}Ga_xAs_yP_{1-y}$ with compositions lattice matched to InP as the substrate crystal. This puts a restriction on the choice of x and y which can be expressed by[3]:

$$y = 2.2020 x/(1 + 0.0659 x).$$
 (2.1)

All the following considerations are confined to the condition of lattice matching.

Most of the material properties which we need for the subsequent calculations are only known for the binary semiconductors constituting the system In-GaAsP. Therefore an interpolation procedure is required to estimate the value Q(x, y) of a particular property for a given quaternary composition, starting from the experimentally known values B(MN) of the respective property of the constituent binary compositions. The most simple approach to calculate Q(x,y) is Vegard's law:

$$Q(x,y) = x y B(GaAs) + x (1 - y) B(GaP) + y (1 - x) B(InAs) + (1 - x) \times (1 - y) B(InP).$$
(2.2)

We use this relation in combination with equation (2.1) to determine most of the quantities needed in calculating n and α . There are, however, exceptions. The bandgap $E_{\rm g}$ as well as the effective mass $m_{\rm e}$ of the electrons have been measured for the whole composition range $y\approx 2.2\,x$ covered by the condition equation (2.1). We are therefore in a position to formulate an analytical relation fitted best to the experimental results for $E_{\rm g}[13]$ and $m_{\rm e}[14,15]$. The functional relation for $m_{\rm e}$ has to be adapted to room temparature since the underlying $m_{\rm e}$ values were measured at low temperatures. Additionally, the Sellmeier coefficients (cf. the following section) and the valence-band split-off energy Δ will be derived from experimental findings.

This can be done by determining m_e for a non-parabolic conduction band as[16]:

$$1/m_e = 1/m_0 + \left\{2P^2/(3\hbar^2)\right\} \left(\frac{2}{E_g} + \frac{1}{E_g + \Delta}\right)$$
 (2.3)

in a first step. m_0 is the electron effective mass at the bottom of the conduction band. P is the matrix element describing the interband interaction. It varies little for different III–V compounds. Δ is the energy separating the degenerate light- and heavy-hole bands at the Γ point from the valence-band branch split off by spin-orbit interaction. $(E_{\rm g}+\Delta)$ is known from experiments for the composition range presently under consideration[13]. Assuming that the dominant temperature influence on m_e originates from $E_{\rm g}$ we find as a first approximation from equation (2.3):

$$1/m_e(T) = 1/m_e(O) - \{2P^2/(3\hbar^2)\}$$

$$\times \left(\frac{2}{E_{\rm g}^2(O)} + \frac{1}{(E_{\rm g}(O) + \Delta)^2}\right) \frac{\Delta E_{\rm g}}{\Delta T} T,$$

where O indicates the respective quantity at low temperatures. The factor comprising the matrix element P can be determined by evaluating equation (2.3) with the low-temperature values. The functional dependence of $m_e(O)$ on composition y can be found by a fit to the experiments. We determine $\Delta E_g/\Delta T$ from the bandgap values at low temperatures and at room temperature. Although this procedure presumably somewhat underestimates the temperature sensitivity of E_g , it should account to some extent for the increasing spin-orbit splitting Δ with increasing temperature T. The composition dependence of $\Delta E_g/\Delta T$ is calculated by the use of equation (2.2). We find the low-temperature value of the bandgap of a quaternary by:

$$E_{\rm g}(O) = E_{\rm g}(T) + (\Delta E_{\rm g}/\Delta T) T$$
,

where T is chosen as 300 K.

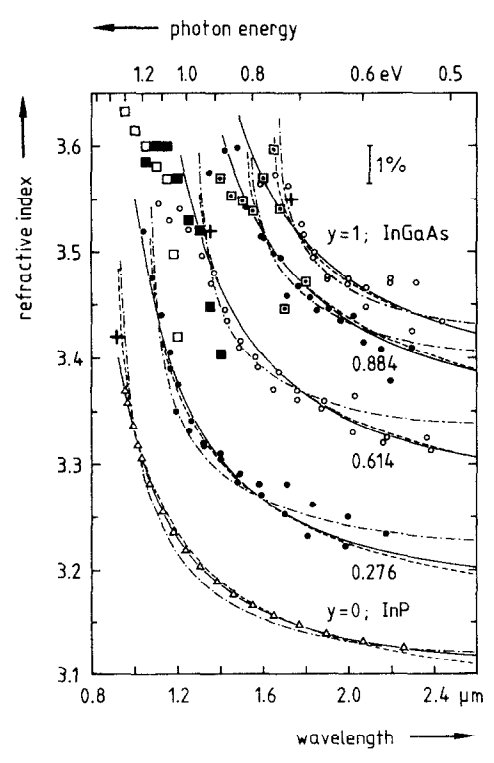
Table 1. Interpolation formulae (last column) used in the present calculations together with the material properties of the constituent binary compounds. All data apply

	to room tem	to room temperature if not stated otherwise. m is the electron mass	stated otherwi	se. m is the	electron mas	SS.	
	Symbol				InP	InP	
Property	(nuit)	GaAs	GaP	InAs	(300 K)	$(77 \mathrm{K})$	$In_{1-x}Ga_xAs_yP_{1-y}/InP$
Bandgap[15]	$E_{\mathbf{g}}(\mathrm{eV})$	1.424	2.272	0.354	1.35	1.4135	$1.35 - 0.72y + 0.12y^2$
Spin-orbit splitting[15]	Δ(eV)	0.34	80.0	0.41	0.11	0.11	$0.119 + 0.30y - 0.107y^2$
$\Delta E_{\rm g}/\Delta T$	(10^{-4} eV/K)	-3	-3.7	-2.1	-2.67		$-2.67 + 0.102y + 0.073y^{2}$
$E_{10} = E_{L,X}^c - E_{\Gamma 6}^c[15]$	(eV)	0.38	-0.508	1.3	0.61	0.9	$0.61 + 0.182y + 0.105y^2$
$E_{20}=E_{\Gamma7}^c-E_{\Gamma6}^c$	(eV)	3.084 [15]	2.6 [15]	4.28	3.38 [19]	3.39 [15]	$3.38 + 0.549y - 0.208y^2$
Deformation potential[22]	$E_{def}(\mathrm{eV})$	6.74	6.1	92.9	7.95	7.95	$7.95 - 2.04y + 0.839y^2$
Effective mass							
Electron (300 K)	m_e/m	0.068	0.33	0.027	0.077	0.069	0.07 - 0.0308y
(low temp.)	$m_e(O)/m$	0.0665	0.21	0.023	<u> </u>	0.0785	$0.0785 + 0.004y - 0.042y^2$
Light holes[15]	m_{hl}/m	0.068	0.16	0.024	0.12	0.12	$0.12 - 0.078_{V} + 0.002_{V}^{2}$
Heavy holes[15]	m_{hh}/m	0.5	0.54	0.41	9.0	9.0	$0.6 - 0.218y + 0.07y^2$
Dielectric constant							
Static[18]	Es	13.18	1:.1	14.55	12.35	12.35	$12.35 + 1.62y - 0.055y^2$
High frequency[19]	ϵ_{σ_c}	10.9	9:036	8.11	9.52	9.52	$9.52 + 2.06y - 0.205y^2$
Sellmeier coefficients	¥	8.95	4.54	7.79	7.255	7.781	$7.255 + 1.15y + 0.489y^2$
	В	2.054	4.31	4.00	2.316	1.661	$2.316 + 0.604y - 0.493y^2$
	Ü	0.39 [21]	0.22 [21]	0.25 [21]	0.3922 [20]	0.4397 [20]	$0.3922 + 0.396y + 0.158y^2$
Density[15]	$\rho(\mathrm{gcm}^{-3})$	5.3161	4.138	2.667	4.81	4.81	4.81 + 0.74v
Longitudinal sound velocity[15] (averaged)	$s(10^5\mathrm{cm/s})$	5.115	6.25	4.351	5.2	5.2	$5.2 - 0.372y - 0.144y^2$
Phonon energy							
LA	$E_{ac}({\sf meV})$	28.1	31	18	24	24	$24 - 2.84y + 1.57y^2$
07	$E_{op}(\mathrm{meV})$	[19] 29.6	[15] 45.4	[19] 20.3	[19] 42.6	[19] 42.6	$42.6 - 21.1y + 2.87y^2$
		[15]	[15]	[61]	[61]	[19]	

Table 1 summarizes the relations found by the procedure as outlined above along with the input data of the binary constituents. These latter data are valid for room temperature [with the exception of $m_e(O)$]. In addition the values measured at liquid-nitrogen temperature with InP are listed which are needed to check the absorption calculations against the experimental results taken at this temperature. The interpolation formulae given in the last column of Table 1 are used in the following calculations.

3. THE REFRACTIVE INDEX

The refractive index n is an important parameter for the design of waveguides, modulators, resonators or lasers. Therefore many attempts were made to derive dependable expressions describing n in dependence on the composition for variable wavelength. Most of these expressions differ only little from each other for wavelengths beyond the bandgap so that it cannot be decided which of them is more accurate given the scatter in the experimental results. This is different in the wavelength range close to the bandgap where some formulae show singularities. We compare the different approaches with the measurements presently available. The details on the calculations are given in Appendix 1.



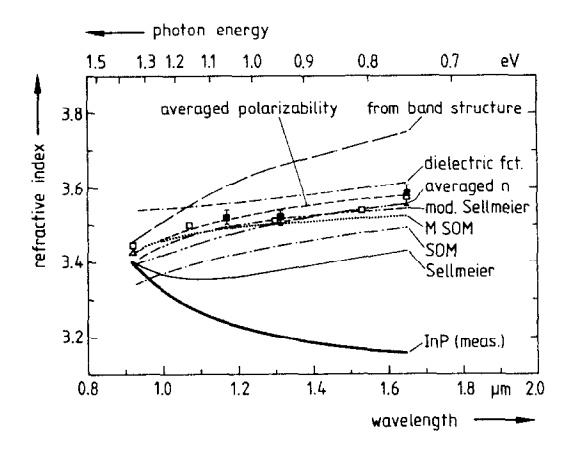


Fig. 2. Refractive index as measured for InP (heavy curve) [20] and as calculated for various models (details see Appendix 1). The calculations were done for varying composition and 5 meV away from the respective E_g value. Experimental points: \Box [5], \triangle [23], \blacksquare [6].

In Figure 1 the experimentally found values of n[5-7,20,31] are displayed in dependence on the wavelength for various compositions. The curves are calculated as outlined in Appendix 1 and were obtained from the modified Sellmeier formula (solid curve), the modified single oscillator model (broken curve) and the dielectric-function calculation (chain curve).

In view of the experimental scatter it is difficult to determine which procedure is more accurate in the wavelength range under consideration. However, all methods show marked singularities close to the bandgap energy. This region is most important for laser applications.

We follow a suggestion by Buus and Adams[21] and plot n, as calculated 5 meV away from $E_{\rm g}$ for varying composition after the different methods as given in Appendix 1, in dependence on the bandgapequivalent wavelength (Fig. 2). We can now compare with the available experiments and find that the method of Burkhard *et al.*[7] describes best the experiments. Also given in Fig. 2 is the measured n for InP[20].

Since in the following we are concerned with the wavelength range well beyond $E_{\rm g}$ we can use the modified Sellmeier formula, which allows convenient calculations, as the basis for the subsequent considerations.

An important influence on n is exerted by free carriers in a semiconductor in the sense that the free-carrier plasma reduces n. This influence is particularly strong for electrons since their effective mass m_e is generally small in III-V compounds. The refractive-index reduction Δn is proportional to the electron concentration N and the square of the free-space wavelength $\lambda[32]$:

$$\Delta n = -N\lambda^2 e^2/(8\pi^2 \epsilon_0 c^2 n m_c), \qquad (3.1)$$

e is the elementary charge and e the velocity of light. A marked effect can be expected for N values beyond

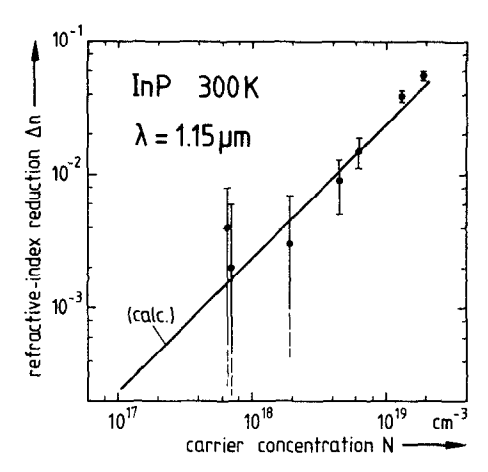


Fig. 3. Change Δn of refractive index in dependence on free-electron concentration N, measured at a wavelength of 1.15 μ m with InP [23]. Solid curve calculated for free-carrier plasma effect.

 10^{18} cm⁻³ which was demonstrated experimentally with InP[23] (Fig. 3). The experiments are very well described by equation (3.1) as shown by the solid line in Fig. 3. We chose n as the low-carrier-concentration value from Ref.[23]. The effect of the free carriers can be used to advantage in the design of waveguides. However, it must be pointed out that increasing carrier concentration goes along with increasing absorption.

4. OPTICAL ABSORPTION

It is evident from the discussion of the preceding section, that experimental data on the refractive index of InGaAsP are relatively scarce. This is even more so when we are now concerned with the optical-absorption coefficient α of which only few measurements are available[6,7,31]. Particularly in the wavelength range beyond the bandgap experiments are completely lacking so that we have to rely for the following calculations on extrapolations from low-temperature data taken with InP[33,38]. The scarcity of experiments is explained by the fact that InGaAsP is available only in the form of epitaxial layers of a thickness not suited for accurate absorption measurements.

The wavelength regime which is of interest for wavelength applications because of its low absorption values is bordered by the high-absorption band-to-band transitions at the short-wavelength side and by the free-carrier absorption at the long-wavelength side (Fig. 4). The direct transitions from the valence band to the conduction band give rise to the absorption contribution α_{VC} . Due to the presence of free carriers in the conduction-band minimum at the Γ point intraband transitions, involving acoustical and optical phonons of the longitudinal branches as well as ionized impurities, can occur. Thus the free-carrier absorption α_{FC} is composed of α_{ac} , α_{op} and α_{imp} . All these absorption coefficients can be calculated by the

use of known material parameters which is not true for the interband absorption α_{IB} dominant in the medium-wavelength range. In principle, the same mechanisms contribute to both α_{IB} and α_{FC} . However, by far the overwhelming influence on α_{IB} stems from the acoustical phonons[34]. In the following we will calculate the total absorption coefficient:

$$\alpha = \alpha_{VC} + \alpha_{IB} + \alpha_{ac} + \alpha_{ap} + \alpha_{imp}$$

where a variable parameter is used to adjust α_{IB} to the experimental finding.

 α_{VC} shows a rapid decline beyond the bandgap which generally can be described by an exponential wavelength dependence[31,35]. By normalizing the measurements taken with GaAs at 90 K and room temperature and with InP at room temperature to the bandgap[35], we find as the best empirical fit:

$$\alpha_{VC} = 3.0 \times 10^3 \exp[-100 (E_g - \hbar \omega)].$$
 (4.1)

To describe the increase of the bandgap by the Burstein shift we employ the relation

$$\Delta E_{\rm g} = 1.6 \times 10^{-8} \, N^{1/3},$$
 (4.2)

where N is the free-electron concentration. Because of the exponential energy dependence equation (4.1), α_{VC} is negligible in the longer wavelength range.

The intraband contributions α_i , where *i* stands for ac, op and imp, were calculated by Haga and Kimura[37] for III-V compounds using a second order perturbation theory. Their result is:

$$\alpha_i = H_i(\hbar \omega/kT) \int_0^\infty G_i(w,z) [f(w) - f(z)] dw, \quad (4.3)$$

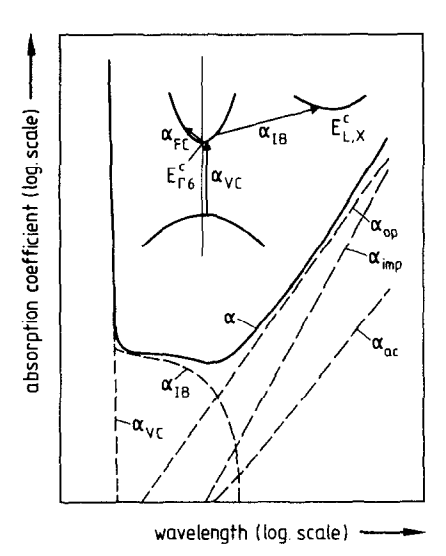


Fig. 4. Schematic representation of the absorption coefficient α in dependence on wavelength in the near-bandgap range. Insert: indication of the transitions involved. α_{VC} direct transition valence to conduction band: α_{IB} indirect inter-conduction-band transition; α_{FC} free-carrier intraband transitions involving acoustical phonons (α_{ac}) , optical phonons (α_{op}) and ionized impurities (α_{imp}) .

where f is the Fermi function and k Boltzmann's constant. w and z have the following meaning:

$$w = E/kT$$

 $z = (E + \hbar\omega)/kT$ for $i = ac$, imp ,
 $z = (E + \hbar\omega \pm E_{ac})/kT$ for $i = ac$.

The factors H_i ($\hbar\omega/kT$) and G_i (w,z) are given in Appendix 2. They contain only material parameters from Table 1 with the exception of the ratio r_c connecting N with the effective impurity concentration by $N_{imp} = r_c N$. r_c is used as an adjustable parameter. The determination of the Fermi energy E_F is also described in Appendix 2.

The interband transitions to the satellite valley in the conduction band (Fig. 4), leading to the absorp- α_{IB} , are—at least contribution GaAs[34]—indirect in the sense that higher lying conduction-band branches are involved as intermediate states for the electrons. One transition of this kind is from the bottom of the conduction band in the Γ point to the next highest energy band at the same point and then to the satellite valley, i.e. the energy difference $E_{20} = E_{\Gamma7}^c - E_{\Gamma6}^c$ applies to the intermediate state. The second transition is from the bottom of the conduction band at Γ to the next highest satellite valley above the final satellite valley at the X or L point as the intermediate state and then down to the lowest satellite valley. In this case the energy difference for the first step is $E_{10} = E_{L,X}^c - E_{\Gamma 6}^c$. Consequently, α_{IR} is composed of two contributions. Since only acoustical phonons have to be included, the result of the calculation is[34]:

$$\alpha_{IB} = A \, m_e^{3/2} \frac{E_{ac} \, E_{def}}{n \rho s^2} \frac{1}{\exp(E_{ac}/kT) - 1}$$

$$\times \frac{1}{(E_{20} - \hbar \omega)^2 \hbar \omega}$$

$$\times \left\{ \exp(E_{ac}/kT) \right.$$

$$\times \left\{ \frac{E^{1/2}(E - E_{10} + \hbar \omega + E_{ac})^{1/2}}{\exp[(E - E_f)/kT] + 1} \, dE \right.$$

$$\left. + \int_{u^-}^{\infty} \frac{E^{1/2}(E - E_{10} + \hbar \omega - E_{ac})^{1/2}}{\exp[(E - E_f)/kT] + 1} \, dE \right\}. \quad (4.4)$$

The lower limits u^{\pm} of the integrals have to be taken as 0 or $(E_{10} - \hbar\omega \mp E_{ac})$ depending on whether $(\hbar\omega \pm E_{ac} - E_{10})$ is positive or negative. The constant A comprises some unknown parameters, notably the matrix element of the momentum operator between the electron states involved. A is treated as an adjustable parameter to fit the experimental results.

We are now in a position to calculate α by exploiting equations (4.1–4.4) in conjunction with Appendix 2. For n we use the modified Sellmeier formula of Appendix 1. The result is shown in Fig. 5. We find r_c by fitting the long-wavelength part of the curves to the experiments taken with InP at liquid-nitrogen temperature [38]. Since r_c in most cases is larger than

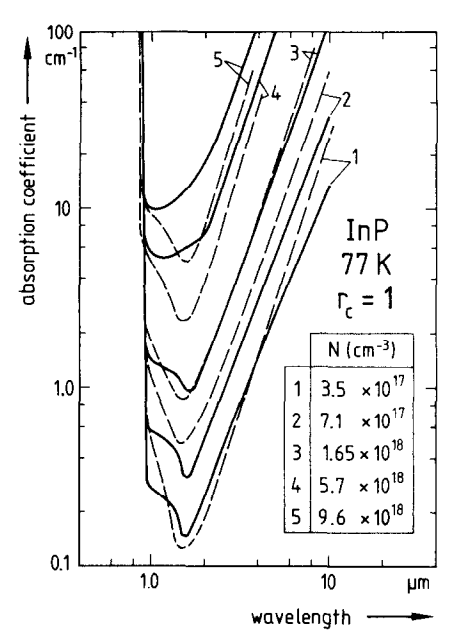


Fig. 5. Absorption coefficient α in dependence on wavelength for InP at liquid-nitrogen temperature. Experiments: broken curves [38]. Solid curves as calculated.

unity[37,39], there must be present an additional absorptive mechanism. In the wavelength range between 1-2 μ m where α_{IB} is dominant we find best agreement with the experiment by choosing $A = 1.4 \times 10^{-5}$. Similar calculations as described above were performed by Jordan for GaAs[39]. Both, the results with GaAs as well as those depicted in Fig. 5, demonstrate that the theoretical treatment presented here is sufficiently accurate in particular for low carrier concentration. The high-doping range where the material is strongly degenerate is of no particular concern for waveguide application. We can be confident that an extrapolation of the calculations to room temperature and to quaternary compositions InGaAsP is a reliable estimate for conditions where almost no measurements are available to date.

In Fig. 6 the calculations for InP are shown as solid curves. They can be compared to measurements in the range beyond $3 \mu m$ where the calculations either closely agree to or deliver larger values than the experiments. At medium wavelengths between $1-2 \mu m$ the calculations are only qualitatively in agreement with the experiments[42] (broken curves) which, however, contrary to all expectation and to all measurements with other III–V compounds show no carrier-concentration dependence at low doping levels.

Figure 7 displays the absorption coefficient in dependence on N for a variety of compositions in the lattice-matched system InGaAsP as estimated for a wavelength of $1.3 \,\mu\text{m}$. We chose $r_c = 1$ in all cases. Since $A = 3.25 \times 10^{-5}$ for GaAs[39], we took $A = (1.4 + 1.85 \,y) \times 10^{-5}$ for the intermediate compositions. The curves for y = 0.45 and in particular for y = 0.5 show the influence of the direct transitions

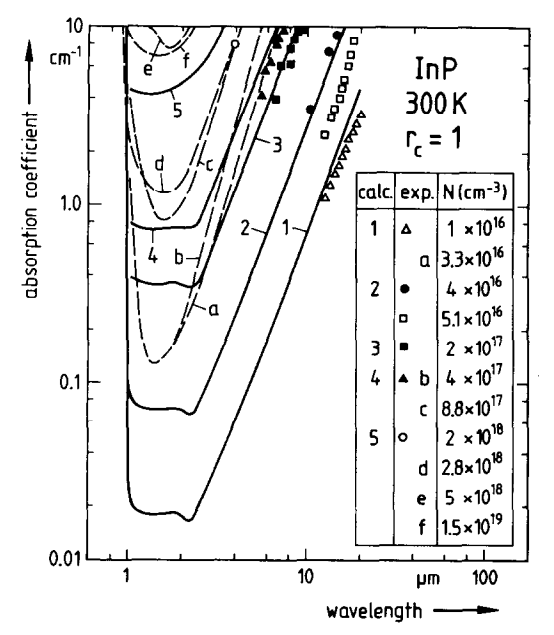


Fig. 6. Absorption coefficient α in dependence on wavelength for InP at room temperature. Experiments: open symbols [40], solid symbols [41]. Broken curves [42]. Solid curves as calculated.

at the band edge close to $1.3 \mu m$. The gradual decline of the 0.5 curve with increasing electron concentration is due to the bandgap widening included in the calculation through equation (4.2). The experimental points were taken with InP[42]. Although they do not show a carrier-concentration dependence in the low doping range as with all other known experiments with III–V compounds they support the calculations.

5. CONSIDERATIONS ON WAVEGUIDES

The radiation propagation in a waveguide suffers losses from a number of sources some of which can

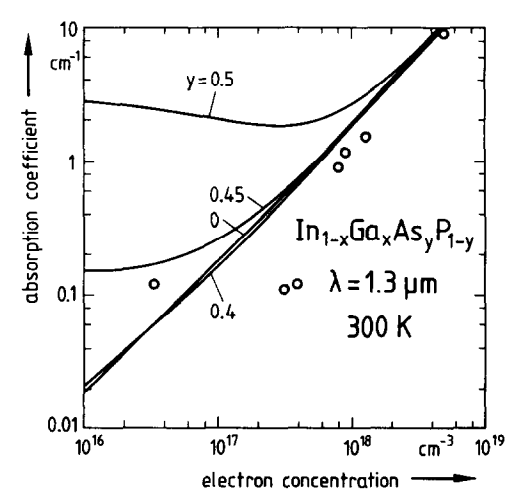


Fig. 7. Absorption coefficient for various compositions InGaAsP in dependence on electron concentration as estimated for a wavelength of $1.3 \, \mu \text{m}$. \bigcirc InP experimental [42].

in principle not be avoided. Among the latter ones is Rayleigh scattering caused by refractive-index fluctuations[43] and depending on the wavelength as λ^{-4} . The attenuation caused by this mechanism can be estimated from the photoelastic constants in the InGaAsP system[44] and the isothermal compressibility. The attenuation found in this way is much too small to be of significance for waveguide dimensions in the present application.

This is different for scattering losses arising from surface or edge irregularities of the waveguide. Even with relatively good dimensional control (roughness around 0.1 µm and correlation length around $10^{-2} \mu m$ as an example) the loss generated by the semiconductor-air interface can amount to several dB/cm[43]. The dependence of the attenuation on the correlation length is weak for the parameters which can be expected for the present application[45]. If, however, the refractive-index step is reduced by embedding the waveguide in semiconductor material of slightly smaller index, the loss can decrease by an order of magnitude since the scattering centers at the interface become proportionately ineffective. This is the reason why generally free surfaces to the waveguide are avoided and why the film-substrate interface contributes much less to the attenuation than the film-vacuum interface even if the roughness of both interface is correlated[45].

In this paper we are concerned with the losses caused by the bulk absorption of the semiconductor. We do not consider losses from mechanical strain or crystal imperfections unless reflected in the exponential wavelength dependence of the direct transitions. As an illustration we discuss first slab waveguides composed of an epitaxial semiconductor film of thickness d on a substrate of slightly smaller refractive index n_s (Fig. 8). We choose $n_s = 3.2$ which applies to InP (Fig. 2). The refractive index n_f of the film, whose upper boundary is to air, is larger than n_s by the amount Δn . Thus the film waves are asymmetric. We consider TE waves of a vacuum wavelength $\lambda = 1.3 \,\mu\text{m}$ having only one component of the electric field in the film plane perpendicular to

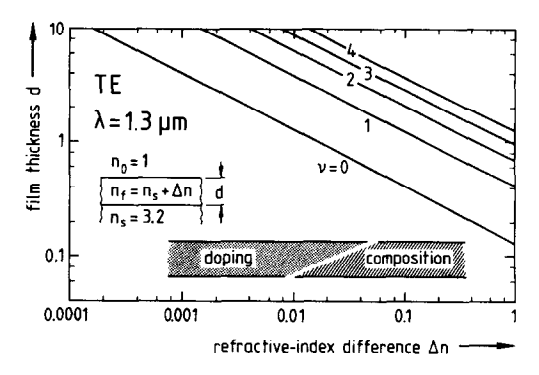


Fig. 8. Cut-off thickness of TE modes with mode number ν in an asymmetric film guide whose refractive index n_f is larger than that of the substrate by Δn .

the propagation direction. From the interference condition deduced from the total reflexion at the film boundaries the minimum film thickness can be calculated which can support waves of mode number v[43]. v specifies how often the field changes sign across the waveguide. The results are displayed in Fig. 8 for the first few modes. The wedges near the abscissa indicate the Δn range which can be covered either by doping of the substrate (Fig. 3) or by change of the composition of the film material (Fig. 1). In both cases the upper limits of Δn are imposed by increasing absorption. The results for TM waves differ from those in Fig. 8 only insofar as slightly smaller cut-off thicknesses are required, particularly for larger Δn values.

We mentioned before that embedded waveguides are preferable in order to reduce loss by surface scattering. Therefore we discuss now a film waveguide as sketched in the insert of Fig. 9. The guiding film whose thickness is d has the composition y = 0.5. Its refractive index $n_1 = 3.44$ at a wavelength of $1.3 \,\mu m$ can be found for example by use of the modified Sellmeier formula or by interpolation from Fig. 1. The absorption coefficient α_1 is around 4 cm⁻¹ in the low doping range (Fig. 7). The substrate and the cover layer are both from InP so that their refractive index is around 3.2 and their absorption coefficient around 0.04 cm⁻¹ (Fig. 7). Since the absorption values are all relatively low (i.e. $\alpha \ll n \ 2\pi/\lambda$) the field distribution in the waveguides is the same as in the completely loss-free case. Therefore we have a cosine distribution within the film and exponential tails in the surrounding media (see e.g. Ref. [43]). By integrating the component of the Poynting vector in the direction of the wave propagation over a sector of the cross-section of the waveguide we can determine the fraction of the total power which passes through this sector. Multiplying this fraction by the relevant absorption coefficient leads to its contribution to the total absorption. We followed this procedure and added the contributions of the guiding film, the substrate and the cover to arrive at the absorption a in Fig. 9. Each curve applies to one particular mode and declines towards the cut-off thickness since the confinement of the mode becomes less stringent. Consequently the relatively large absorption in the guiding film is of decreasing influence.

For practical devices a guiding mechanism in the

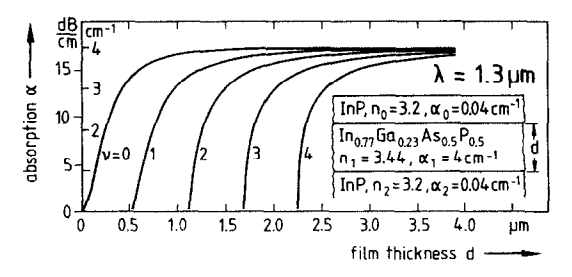


Fig. 9. Absorption, originating from bulk absorption, as calculated for a film waveguide at a wavelength of 1.3 μ m. ν is the mode number.

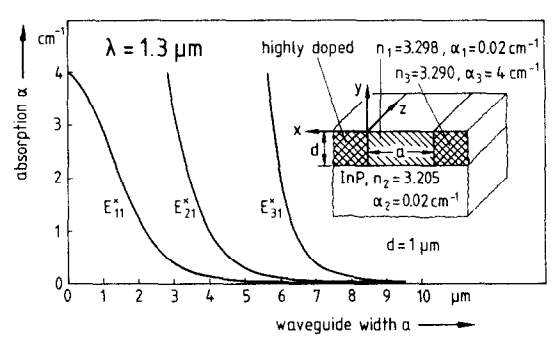


Fig. 10. Absorption of a diffused waveguide for modes of polarization essentially in the x direction. The composition of the epitaxial film is y = 0.2.

film plane must be provided leading to a strip waveguide. A large number of different strip waveguides, mainly based on GaAs, have been reported in the literature[32,46]. For strip waveguides scattering losses, introduced by rough interfaces and neglected in the previously discussed example, are of particular concern so that the structure of the guide must be carefully selected.

As an example we discuss the structure depicted in the insert to Fig. 10. This waveguide minimizes losses introduced by geometric irregularities, in particular if it is fabricated by employing a growth technique like metal-organic vapour-phase epitaxy which leads to very flat surfaces. Therefore we can concentrate on the losses caused by the absorption of the bulk material alone. The basis for the waveguide of Fig. 10 is n doped InP $(10^{16} \,\mathrm{cm}^{-3})$ serving as a substrate for a quaternary layer of composition y = 0.2 $(\lambda_g = 1 \,\mu\text{m})$, of thickness of $1 \,\mu\text{m}$ and of an electron concentration of 1016 cm⁻³. For both materials we find from Fig. 7 the absorption coefficient $\alpha_1 = \alpha_2 = 0.02$ cm⁻¹. From the modified Sellmeier formula (Table 1) we find as refractive index the value 3.205 for the substrate and 3.298 for the quaternary film at the operating wavelength of $1.3 \mu m$. The reduction of the refractive index by the free-carrier effect can be neglected. To assure a sufficiently strong lateral guiding, required especially for bends, the relevant refractive-index step must be high. Because of their large effective mass this cannot be easily realized by holes particularly in view of the limited acceptor-concentration attainable by commonly used diffusion[47]. Moreover, p-type material displays generally much larger absorption than n-type material[48]. On the other hand, if an electron concentration of $2 \times 10^{18} \,\mathrm{cm}^{-3}$ is introduced by ion implantation, e.g. of Si, the refractive-index reduction of 0.008 necessary for lateral guiding can be provided. This leads to an absorption of $\alpha_3 = 4 \text{ cm}^{-1}$ in the regions surrounding the waveguide (Fig. 7). In order to estimate the absorption of the waveguide we apply the method by Marcatili[49] to obtain the field distribution. The absorption can then be found as in the case of the slab waveguide by adding up all the

contributions from the various sectors of the structure.

The result is displayed in Fig. 10 in dependence on the waveguide width a for the family of guided modes whose polarization is essentially in the x direction, i.e. the main component E_{ii}^x of the electric field is perpendicular to the propagation direction z in the film plane as indicated by the upper index x. As expected for the structure, sketched in the insert of Fig. 10, the guided modes are hybrid. Their field distribution is sinusoidal within the guide[49] with the lower indices i and j giving the number of extrema in the x and ydirection, respectively. Outside the guiding region the field decays exponentially. It may be observed that the structure is monomodal in the y direction which might also be inferred from Fig. 8 for the given film thickness of $1 \mu m$. The attenuation of the modes decreases from 4 cm⁻¹, dominated by the absorption coefficient of the highly doped regions at weak guiding (small transverse dimension a), to smaller values at increasing light confinement to the low-loss region of the waveguide (increasing a).

6. CONCLUSIONS

The quaternary semiconductor InGaAsP with compositions lattice matched to InP as a substrate can be used to design active and passive devices for the wavelength range around $1.3-1.5\,\mu\mathrm{m}$. Therefore it is of paramount importance for optical communication systems employing glass fibres. In particular, InGaAsP can be utilized for optical waveguides which are essential components in future optical integrated circuits based on InP. The refractive index n and the optical absorption coefficient α are the parameters dominating the performance of the waveguides.

We demonstrate that n can be described analytically for the compositions in question by a modified Sellmeier formula which, however, breaks down near the bandgap. Here the procedure, interpolating the polarizability of the binary constituents of the system InGaAsP[7], agrees best with the experiments. Besides changing n by varying the composition of InGaAsP and thus the bandgap, an alternative method is the increase of the free-carrier concentration which effectively reduces n.

As to the absorption coefficient α , complex bandstructure considerations can be exploited to estimate its lowest level in the wavelength range between the fundamental absorption at the band edge and the increasing free-carrier effect towards longer wavelength. Although only few experiments were reported and, moreover, these were taken at low temperatures, the agreement with the calculations is good enough to give credibility to an extrapolation to room temperature. Accordingly, α values well below 1 cm⁻¹ should be attainable by proper choice of composition. The results can then be used to determine the modes propagating along an optical waveguide, which is done for a slab waveguide and for a somewhat idealized form of a diffused waveguide. We show that in both cases α values of 1 cm⁻¹ or less are realizable. This view is corroborated by the scarce relevant experiments which revealed α values around 1.5 cm⁻¹ for InP-based waveguides[50]. Since GaAs in all basic aspects is similar to InP and since GaAs-based waveguide losses of 0.2 dB/cm were measured[51], much lower α values can be expected also with InP. It is important, though, that losses caused by surface irregularities are avoided by suitable design of the waveguide.

It can be concluded that according to the present investigations the quaternary system InGaAsP/InP can be used to advantage for optical waveguides. However, it is evident that there is still a great lack of experimental data in the range of low optical absorption.

Acknowledgements—The authors are indebted to I. Kneppo, D. Wittenburg and particularly to G. Hoppe for substantial help at various stages of the calculations performed for this paper. They would like to express their gratitude to an anonymous referee whose constructive criticism led to the removal of a weakness of the original manuscript.

REFERENCES

- Y. Suematsu (Editor), Optical Devices and Fibers. North Holland, Amsterdam (1983).
- P. Kaiser, Proc. 5th Int. Conf. Integrated Optics and Opt. Fiber Commun., 11th Eur. Conf. Opt. Commun., Venice, Vol. 2, p. 125 (1985).
- 3. T. P. Pearsall (Editor), GalnAsP Alloy Semiconductors. Wiley, New York (1982).
- P. Buchmann, H. Kaufmann, H. Melchior and G. Guekos, In: *Integrated Optics* (Edited by H. P. Nolting and R. Ulrich), p. 135. Springer, New York (1985).
- P. Chandra, L. A. Coldren and K. E. Strege, Electron. Lett 17, 6 (1981).
- W. Kowalsky, H.-H. Wehmann, F. Fiedler and A. Schlachetzki, *Physica Status Solidi* 77a, K75 (1983).
- H. Burkhard, H. W. Dinges and E. Kuphal, J. appl. Phys. 53, 655 (1982).
- 8. T. M. Benson, T. Murotani, P. N. Robson and P. A. Houston, *Proc. Integrated Optics Conf.*, London, paper 9. 4-1 (1981).
- K. Tada and N. Suzuki, Jap. J. appl. Phys. 19, 2295 (1980).
- H. G. Bach, J. Krauser, H. P. Nolting, R. A. Logan and F. K. Reinhart, Appl. Phys. Lett. 42, 692 (1983). A. Carenco, H. Menigaux and N. T. Linh, Appl. Phys. Lett. 40, 653 (1982).
- O. Mikami and H. Nakagome, *Electron. Lett.* 20, 228 (1984).
- S. Aytac and A. Schlachetzki, J. Opt. Commun. 6, 82 (1985).
- R. E. Nahory, M. A. Pollack, W. D. Johnston and R. L. Barns, Appl. Phys. Lett. 33, 659 (1978). M. A. Pollack, R. E. Nahory, J. C. DeWinter and A. A. Ballman, Appl. Phys. Lett. 33, 314 (1978). H. H. Caspers and H. H. Wieder, Solid State Commun. 29, 403 (1979). E. H. Perea, E. E. Mendez and C. G. Fonstad, Appl. Phys. Lett. 36, 978 (1980). P. M. Laufer, F. H. Pollack, R. E. Nahory and M. A. Pollack, Solid State Commun. 36, 419 (1980). R. Madelon and M. Dore, Solid State

- Commun. 39, 639 (1981). Y. Yamazoc, T. Nishino and Y. Hamakawa, IEEE J. Quantum Electron. QE-17, 139 (1981)
- J. B. Restorff, B. Houston, J. R. Burke and R. E. Hayes, Appl. Phys. Lett. 32, 189 (1978). R. J. Nicholas, J. C. Portal, C. Houlbert, P. Perrier and T. P. Pearsall, Appl. Phys. Lett. 34, 492 (1979). H. Brendecke, H. L. Störmer and R. J. Nelson, Appl. Phys. Lett. 35, 772 (1979). R. J. Nicholas, S. J. Sessions and J. C. Portal, Appl. Phys. Lett. 37, 178 (1980). E. H. Perea, E. Mendez and C. G. Fonstad, J. Electron. Mat. 9, 459 (1980).
- Landolt-Börnstein, Numerical Data and Functional Relationships in Science and Technology, (Series edited by K.-H. Hellwege), vol. 17, (Volume edited by O. Madelung, M. Schulz and H. Weiss). Springer, Berlin (1982).
- W. Zawadzki, In: Handbook on Semiconductors, (Edited by T. S. Moss), Vol. 1, Chap. 12. North Holland, Amsterdam, (1982).
- F. P. Kesamanly, D. N. Nasledov, A. Ya, Nashel'skili and V. A. Skripkin, Sov. Phys. Semicond. 2, 1221 (1969).
- E. E. Klotyn'sh and V. K. Petrov, Sov. Phys. Semicond.
 370 (1975). A. Raymond, J. L. Robert and C. Bernard, J. Phys. C: Solid State Phys. 12, 2289 (1979).
- M. Neuberger, Handbook of Electronic Materials— III-V Semiconducting Compounds, Vol. 2 IFI/Plenum, New York (1971).
- G. D. Pettit and W. J. Turner, J. appl. Phys. 36, 2081 (1965).
- J. Buus and M. J. Adams, Solid-St. Electron Dev. 3, 189 (1979).
- 22. S. Adachi, J. appl. Phys. 53, 8775 (1982).
- M. S. Whalen and J. Stone, J. appl. Phys. 53, 4340 (1982).
 J. Stone and M. S. Whalen, Appl. Phys. Lett. 41, 1140 (1982).
- 24. T. Takagi, Jap. J. appl. Phys. 21, L 167 (1982).
- 25. K. Utaka, K.-I. Kobayashi and Y. Suematsu, IEEE J. Quantum Electron. QE-17, 651 (1981).
- 26. M. A. Afromowitz, Solid State Commun. 15, 59 (1974).
- 27. S. Adachi, J. appl. Phys. 53, 5863 (1982).
- R. E. Nahory and M. A. Pollack, Electron. Lett. 14, 727 (1978).
 G. H. Olson, T. Z. Zamerowski, P. T. Smith and E. P.
- G. H. Olsen, T. Z. Zamerowski, R. T. Smith and E. P. Bertin, J. Electron. Mat. 9, 977 (1980).
- 30. B. Jensen and A. Torabi, J. appl. Phys. 54, 3623 (1983).
- W. Kowalsky, A. Schlachetzki and F. Fiedler, *Physica Status Solidi* 68(a), 153 (1981).
- 32. R. G. Hunsperger, Integrated Optics: Theory and Technology, Optical Sciences Vol. 33. Springer, Berlin (1982).
- M. R. Lorenz, W. Reuter, W. P. Dumke, R. J. Chicotka, G. D. Pettit and J. M. Woodall, *Appl. Phys. Lett.* 13, 421 (1968).
- 34. E. Haga and H. Kimura, J. Phys. Soc. Jap. 19, 1596 (1964).
- R. K. Willardson and A. C. Beer (Editors), Semiconductors and Semimetals, Vol. 3. Academic Press, New York (1967).
- 36. N. K. Dutta, J. appl. Phys. 51, 6095 (1980).
- E. Haga and H. Kimura, J. Phys. Soc. Jap. 19, 658 (1964).
- 38. W. P. Dumke, M. R. Lorenz and G. D. Pettit, *Phys. Rev.* **B1**, 4668 (1970).
- 39. A. S. Jordan, J. appl. Phys. 51, 2218 (1980).
- M. Yamaguchi, A. Yamamoto, S. Shinoyama and H. Sugiura, J. appl. Phys. 53, 633 (1982).
- 41. R. Newman, Phys. Rev. 111, 1518 (1958).
- A. A. Ballman, A. M. Glass, R. E. Nahory and H. Brown, J. Crystal Growth 62, 198 (1983).
- 43. H.-G. Unger, *Planar Optical Waveguides and Fibers*. Oxford University Press, Oxford (1977).
- 44. N. Suzuki and K. Tada, Jap. J. appl. Phys. 22, 441 (1983).
- 45. G. H. Ames and D. G. Hall, *IEEE J. Quantum Electron*. **QE-19**, 845 (1983).

- T. Tamir (Editor), *Integrated Optics*, 2nd edn. Springer, Berlin (1979).
- 47. S. Aytac and A. Schlachetzki, J. Crystal Growth 64, 169 (1983).
- 48. C. H. Henry, R. A. Logan, F. R. Merritt and J. P. Luongo, *IEEE J. Quantum Electron*. **QE-19**, 947 (1983).
- 49. E. A. J. Marcatili, Bell Syst. Techn. J. 48, 2071 (1969).
- C. Bornholdt, W. Döldissen, D. Franke, N. Grote, J. Krauser, U. Niggebrügge, H. P. Nolting, M. Schlak and I. Tiedke, *Electron. Lett.* 19, 81 (1983). P. Buchmann and A. J. N. Houghton, *Electron. Lett* 18, 850 (1982).
- K. Ishida, K. Hiruma, H. Inoue, T. Asai, M. Hirao and H. Matsumura, Eur. Conf. Int. Optics, Berlin, paper P4 (1985).

APPENDIX 1: METHODS OF CALCULATING THE REFRACTIVE INDEX

(A) Sellmeier formula

The classic Sellmeier formula describes n near the resonance of a mechanism set in motion by the light wave. The formula [21,23] can be used for all compositions y by inserting the Sellmeier coefficients, as given in Table 1, into:

$$n^{2}(\lambda) = \sum_{i=1}^{4} [A_{i} + (B_{i}\lambda^{2})/(\lambda^{2} - C_{i})]f_{i}.$$

 λ is the wavelength and *i* refers to the four binary constituents of the system. The respective weighting factors f_i can be taken from equation (2.2). However, the physical quantity to average is not the refractive index, but rather the oscillator characteristics. This leads us to:

$$n^2 = A + B\lambda^2/(\lambda^2 - C),$$

where A, B and C are taken as the interpolated values from Table 1. We call this the modified Sellmeier formula.

(b) Single oscillator model (SOM)

The single oscillator model employs two adjustable parameters which might be termed oscillator energy E_o and dispersion energy E_d [24]. n can be found from:

$$n^2 = 1 + (E_o E_d)/[E_0^2 - (\hbar \omega)^2],$$

where \hbar is Planck's constant divided by 2π and ω is the angular frequency of the light. For our calculations we use the expressions [25]:

$$E_o = 3.391 - 1.652y + 0.863y^2 - 0.123y^3,$$

 $E_d = 28.91 - 9.278y + 5.626y^2.$

(c) Modified single-oscillator model (MSOM)

Both the Sellmeier method as well as the SOM neglect absorption and therefore are only applicable away from the resonance. The modified single-oscillator model[26] uses a more realistic approach for the absorption leading to:

$$\begin{split} n^2 &= 1 + E_d/E_o + E_d (\hbar\omega)^2/E_0^3 + \frac{E_d}{2E_0^3(E_0^2 - E_g^2)} \\ &\times (\hbar\omega)^4 \ln \left[\frac{2E_0^2 - E_g^2 - (\hbar\omega)^2}{E_g^2 - (\hbar\omega)^2} \right] \end{split}$$

(d) Dielectric function calculation

Adachi[27] calculates the imaginary part of the dielectric function for direct band-to-band and Wannier-exciton transitions which latter mechanism is of little significance. By exploiting the Kramers-Kronig relations, n is obtained as:

$$n^{2} = (8.4 - 3.4y) \{ g (\hbar \omega / E_{g}) + \frac{1}{2} [E_{g} / (E_{g} + \Delta)]^{3/2}$$

$$\times g [\hbar \omega / (E_{g} + \Delta)] \} + 6.6 + 3.4y$$

with

$$g(x') = [2 - (1+x')^{1/2} - (1-x')^{1/2}]x'^{-2}.$$

(e) Interpolation of polarizabilities

Several authors attempted to calculate n for different compositions near their bandgap by the use of Vegard's law, equation (2.2). Nahory and Pollack [28] arrive at:

$$n \approx 3.4 + 0.256y - 0.095y^2$$

whereas Olsen et al.[29] find:

$$n = 3.39 + 0.207y - 0.043y^2.$$

This procedure is physically unjustified. Instead the atomic polarizability is the physical quantity which can be averaged. This has been done by Burkhard *et al.*[7] with the result:

$$n = 3.425 + 0.94(\hbar\omega - E_g) + 0.952(\hbar\omega - E_g)^2 + [0.255 - 0.257(\hbar\omega - E_g)]y - [0.103 - 0.0952(\hbar\omega - E_g)]y^2.$$

This relation is valid for the energy range 0.2 eV below $E_{\rm e}$.

(f) Calculation from band-structure parameters

A quantum mechanical treatment starting from the band structure of III-V compounds and involving only parameters such as E_g , m_e , m_{bh} , Δ , lattice constant and carrier concentration leads to values of the refractive index with no adjustable constants. In Fig. 2 we display the results obtained by this procedure as described in Ref. [30].

APPENDIX 2: INTRABAND ABSORPTION COEFFICIENTS AND FERMI ENERGY

The factors to be used in equation (4.3) for polar crystals are the following [37]:

for acoustical phonon interaction:

$$H_{ac} = \frac{2e^2m_e^2kTE_{def}^2}{3\pi^3\epsilon_0\hbar^5cn\rho s^2} \left(\frac{kT}{\hbar\omega}\right)^3$$

$$G_{ac} = [E(E+\hbar\omega)]^{1/2}(2E+\hbar\omega)/(kT)^2;$$

for optical phonon interaction:

$$\begin{split} H_{op} &= \frac{e^4 m_e E_{op}}{24 \pi^3 \epsilon_0^2 \hbar^3 cn k T} \left(\frac{1}{\epsilon_{\infty}} - \frac{1}{\epsilon_s} \right) \left(\frac{kT}{\hbar \omega} \right)^3 \\ &\times \frac{\sinh \left\{ \hbar \omega / (2 \, kT) \right\}}{\sinh \left[E_{op} / (2 \, kT) \right] \sinh \left[(\hbar \omega \pm E_{op}) / (2 \, kT) \right]} \\ G_{op} &= 2 [E \left(E + \hbar \omega \pm E_{op} \right)]^{1/2} \\ &\times \left(1 + \frac{(g \, kT)^2}{(2 \, E + \hbar \omega \pm E_{op} + g \, kT)^2} \right) / kT \\ &- 4 E \left(E + \hbar \omega \pm E_{op} \right) \right]^{1/2} \\ &- g \ln \left\{ \frac{2 \, E + \hbar \omega \pm E_{op} + g \, kT}{+ 2 [E \left(E + \hbar \omega \pm E_{op} \right)]^{1/2}} \right\} \\ &- 2 [E \left(E + \hbar \omega \pm E_{op} \right)]^{1/2} \end{split}$$

for impurity interaction:

$$\begin{split} H_{imp} &= \frac{e^{\delta} N_{imp}}{6 \pi^{3} \epsilon_{0}^{3} \hbar c n \epsilon_{s}^{2} (kT)^{2}} \bigg(\frac{kT}{\hbar \omega} \bigg)^{3} \\ G_{imp} &= \frac{1}{4} \ln \left\{ \frac{2E + \hbar \omega + gkT + 2[E(E + \hbar \omega)]^{1/2}}{2E + \hbar \omega + gkT - 2[E(E + \hbar \omega)]^{1/2}} \right\} \\ &- \frac{gkT[E(E + \hbar \omega)]^{1/2}}{(2E + \hbar \omega + gkT)^{2} - 4E(E + \hbar \omega)}. \end{split}$$

The function g is defined as:

$$g = \frac{e^2 (2m_e)^{1/2}}{2\pi^2 \epsilon_0 \epsilon_s \hbar kT} \int_0^\infty E^{1/2} \left(-\frac{\partial f}{\partial E} \right) dE.$$

Besides the quantities already defined above, e.g. in Table 1, ϵ_0 as the permittivity of the free space are used. For α_{op} both contributions (with the plus and minus sign) have to be determined and added.

The Fermi energy E_F can be found from the carrier concentration N which is given as the integral of the density of states weighted by the Fermi function. The result for a nonparabolic band structure is[16]:

$$N = \frac{1}{2\pi^2} \left(\frac{2m_e}{\hbar^2 E_g} \right)^{3/2} \int_0^{\infty} \frac{(2E + E_g)(E^2 + EE_g)^{1/2}}{\exp[(E - E_F)/kT] + 1} dE$$

where the lower limit of the integration is the bottom of the conduction band which is at the same time zero for the energy scale.